Available online at www.sciencedirect.com
SCIENCE DIRECT®
Sensors and Actuators A 121 (2005) 253–261
SENSORS AND ACTUATORS A PHYSICAL
www.elsevier.com/locate/sna

A MEMS multi-sensor chip for gas flow sensing

Yong Xu[a,*], Chen-Wei Chiu[b], Fukang Jiang[b], Qiao Lin[c], Yu-Chong Tai[d]

[a] *Electrical and Computer Engineering, 5050 Anthony Wayne Dr., Wayne State University, Detroit, MI 48202, USA*
[b] *Umachines Inc., Altadena, CA 91001, USA*
[c] *Mechanical Engineering, Carnegie Mellon University, Pittsburgh, PA 15213, USA*
[d] *Electrical Engineering, California Institute of Technology, Pasadena, CA 91125, USA*

Received 3 February 2004; accepted 6 December 2004
Available online 2 February 2005

Abstract

This paper reports the development of a MEMS multi-sensor chip that enables the simultaneous measurements of shear stress, pressure, and temperature inside microchannels. On the multi-sensor chip, five sensor clusters, which consist of shear-stress, pressure, and temperature sensors, are arranged in a one-dimensional array. The multi-sensor chip has been characterized in a rectangular microchannel using both incompressible and compressible gas flows. A simple normalization method has proven to be effective in the reduction of the sensitivity variation of the shear-stress sensors. It has also been found out that the classical theory for conventional hot-film sensors needs to be modified for the MEMS thermal shear-stress sensors. Furthermore, flow rate measurements based on both differential pressure and thermal anemometry principles have been demonstrated using the multi-sensor chip.

Keywords: Flow sensor; Shear-stress sensor; Pressure sensor; Temperature sensor; Microchannel flow

1. Introduction

The measurement of wall shear-stress, pressure, and temperature distributions is of great interest for many fluidic applications. However, this is a very challenging task for the measurement of flows inside a microchannel. MEMS technology enables the fabrication of arrays of miniaturized shear-stress, pressure, and temperature sensors [1–3] and thus enables flow measurement inside microchannels. The first ever experimental data of the pressure distribution of gaseous flows in microchannels using MEMS technology were reported by Liu et al. [4]. Several groups have studied the temperature change/distribution inside microchannels [5,6]. For channels with uniform cross-sectional areas, the wall shear stress can be derived from the pressure gradient. But for channels with non-uniform cross-sectional areas, e.g., nozzles, it is highly desirable to measure both shear stress and pressure directly. This paper reports the first MEMS multi-sensor chip that enables the simultaneous measurement of shear-stress, pressure, and temperature distributions of microchannel flows. Compatible sensor designs have been implemented that simplifies the fabrication of the multi-sensor chip. The fabricated multi-sensor chip has been successfully tested with both incompressible and compressible channel flows. In addition, flow rate measurements have been demonstrated.

2. Sensor designs

Intuitively, the wall shear stress can be determined directly by measuring the force exerted on a small surface area. The micromachined versions of direct measurement have been realized by using floating elements [7–10]. The wall shear stress can be determined from the displacement of the floating element or the force it experiences. Alternatively, shear stress can be measured indirectly using the Stanton tube, Preston tube, sublayer fence, or techniques that are based on electrochemical or thermal principles [11]. Among these

* Corresponding author. Tel.: +1 313 577 3850; fax: +1 313 577 1101.
E-mail address: yxu@ece.eng.wayne.edu (Y. Xu).

0924-4247/$ – see front matter © 2004 Elsevier B.V. All rights reserved.
doi:10.1016/j.sna.2004.12.022

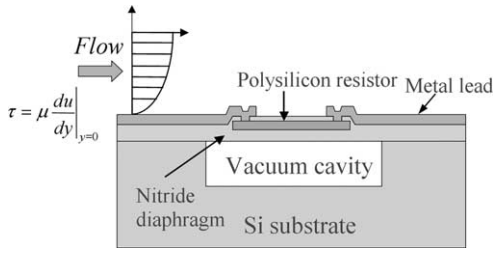

Fig. 1. The cross-section of the micromachined thermal shear-stress sensor.

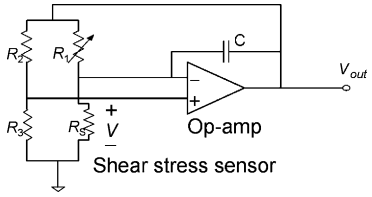

Fig. 2. Simplified constant temperature (CT) bias circuit. R_S is the shear-stress sensor; R_1, R_2 and R_3 are off-chip resistors.

approaches, the thermal method is most frequently used despite its non-linear output. This is mainly because the thermal method has the advantages that it can be used in a wide variety of flows, it does not interfere with the flow, and it offers the possibility of measuring time-varying flows. Additionally, thermal methods are well suited to micromachining, allowing for MEMS shear-stress sensors without moving parts.

Conventional thermal shear-stress sensors are typically made by depositing thin metal film resistors, mostly platinum or nickel, on flat substrates. With the MEMS technology, novel thermal shear-stress sensors have been successfully developed [12–14]. As shown in Fig. 1, the sensor consists of a polysilicon resistor embedded in a nitride diaphragm with a vacuum cavity underneath. Heat loss to substrate is significantly reduced and the heated area is confined to a small area, leading to a much better spatial resolution. The input power of the resistor is a function of the wall shear stress of the ambient fluid, which is defined by:

$$\tau = \mu \left.\frac{\mathrm{d}U}{\mathrm{d}y}\right|_{y=0} \tag{1}$$

where μ is the fluid viscosity, U the streamwise velocity and y-axis is normal to and originates at the sensor surface. The relationship between τ and the input power P to the sensor is typically described by [15]:

$$P = \frac{V^2}{R_S} = \Delta T(A(\rho\tau)^{1/3} + B) \tag{2}$$

where V and R_S are the voltage and electrical resistance of the shear-stress sensor, respectively, ΔT the average temperature difference between the heated resistor and ambient, $A \propto C_p^{1/3} k_T^{2/3}/\mu^{1/3}$ (C_p and k_T are the heat capacity and thermal conductivity of the fluid, respectively), ρ the density of the fluid and the term B represents the heat loss to the substrate and is a function of the dimension and thermal conductivity of the diaphragm. The physical interpretation of Eq. (2) is that the Joule heating generated dissipates in two ways: the convection loss to ambient fluid and the conduction loss to the substrate. Radiation loss is negligible at the typical operating temperature. Note that Eq. (2) is derived for conventional hot-film sensors. As will be shown later, the exponent of τ is not 1/3 for our micromachined shear-stress sensors. Thus, we will use the empirical formula

$$P = \frac{V^2}{R_S} = \Delta T(A_t(\rho\tau)^{1/n} + B_t) \tag{3}$$

where A_t, B_t, and n are determined experimentally.

The shear-stress sensor can operate in either constant temperature (CT) mode or constant current (CC) mode. CT mode is chosen in this work because of its high sensitivity. Fig. 2 shows the simplified CT biasing circuits, where R_S is the shear-stress sensor, R_1, R_2, and R_3 are off-chip resistors that have nearly zero temperature coefficient of resistance (TCR). Here, the resistance of R_2 is chosen to be equal to the resistance of R_3. R_S, R_1, R_2, and R_3, together with the operational amplifier, form a negative feedback loop, which requires that R_S must be equal to R_1 when steady state is reached. An important parameter for the operation of shear-stress sensor is the (resistive) over-heat ratio, which is defined as

$$a_R = \frac{R_S - R_{S0}}{R_{S0}} \tag{4}$$

where R_S is the resistance of the shear-stress sensor at the operating temperature and R_{S0} is the resistance at a reference temperature. For example, if an over-heat ratio of 10% is desired, we then set $R_1 = (1 + 10\%)R_{S0}$. The Joule heating will increase the temperature of shear-stress sensor and thus its resistance (positive TCR). Finally the Wheatstone bridge is balanced and $R_S = R_1 = (1 + 10\%)R_{S0}$. By measuring V_{out} or V ($V_{out} = 2V$), we know how much power is dissipated through fluid and hence the shear stress.

The temperature sensor is a polysilicon thermistor, taking advantage of the temperature dependence of polysilicon's electrical resistivity [16]. The resistance R at temperature T is given by:

$$R = R_0[1 + \alpha_T(T - T_0)] \tag{5}$$

where R_0 is the resistance at a reference temperature T_0 and α_T is the temperature coefficient of resistance of polysilicon.

The pressure sensor is also constructed by embedding polysilicon resistors in a vacuum-sealed nitride diaphragm. In this case, the polysilicon thin films are employed as piezoresistors and are placed at the edge and central areas of the diaphragm where the maximum stress occurs [17]. The pressure is detected by measuring the resistance change of the piezoresistors in the form of a Wheatstone bridge. The resis-

tance change of the polysilicon piezoresistors is given by:

$$\frac{\Delta R}{R} = G_l \varepsilon_l + G_t \varepsilon_t \quad (6)$$

where G_l and G_t are longitudinal and transverse gauge factors of polysilicon, ε_l and ε_t are the average longitudinal and transverse strains.

3. Fabrication

The multi-sensor chip contains five sensor clusters arranged in 1D array, with a pitch of 2 mm, consisting of shear-stress, pressure, and temperature sensors. The nitride diaphragms of both shear-stress and pressure sensors are chosen to be 210 μm × 210 μm. The sensing element of the shear-stress sensor is a straight polysilicon resistor (7 μm wide and 150 μm long) with a typical resistance of 1.4 kΩ at the room temperature (Fig. 4). For pressure sensors, serpentine polysilicon resistors, which form a Wheatstone bridge, are placed on the edge and center of the diaphragm. The temperature sensor is designed as an annular polysilicon thermistor with a typical resistance of 4 kΩ. It is worth noting that the sensing elements of the shear-stress, pressure, and temperature sensors are all made from thin film polysilicon. The simplified fabrication process of the multi-sensor chip is shown in Fig. 3. The process starts with the deposition of 0.2 μm silicon nitride layer in a low pressure chemical vapor deposition (LPCVD) furnace at 830 °C. Note that the resulting thin film is silicon-rich nitride with Si to N ratio close to 1 and the stress is much lower (<300 MPa) than the stoichiometric Si_3N_4 [18]. The nitride layer is then patterned with fluorine-based plasma and 1 μm deep trenches are formed by further etching into silicon. Thermal oxide is grown to fill the trenches, and then the wafer is planarized by HF dip. A 0.4 μm thick phosphosilicate glass (PSG) layer is deposited, densified at 1050 °C, and patterned by Buffer HF (BHF) to form the etch channels. The densification step is required to avoid irregular edges during BHF etch. Next, about 1.5 μm thick low-stress nitride layer is deposited and patterned to open the etch holes. PSG and thermal oxide are removed by 48% HF through etch holes and the nitride diaphragms are released. After this, the cavities are sealed by depositing another layer of low-stress nitride. A 0.5 μm thick polysilicon film is then deposited, doped, annealed, and patterned to form the sensing elements of all the three types of sensors. Note that the polysilicon is doped twice. The first doping is a global boron ion implantation with a dose of $1 \times 10^{15}\,cm^{-2}$, resulting in a doping concentration of $2 \times 10^{19}\,cm^{-3}$. The second doping is a selective high-dose boron ion implantation with a dose of $1 \times 10^{16}\,cm^{-2}$ (leading to a doping concentration of $2 \times 10^{20}\,cm^{-3}$) on the shear-stress, temperature sensors and also on the contacts and turning sections of the pressure resistors to minimize the connection resistance. Although polysilicon resistors are employed as sensing elements for all three types of sensors,

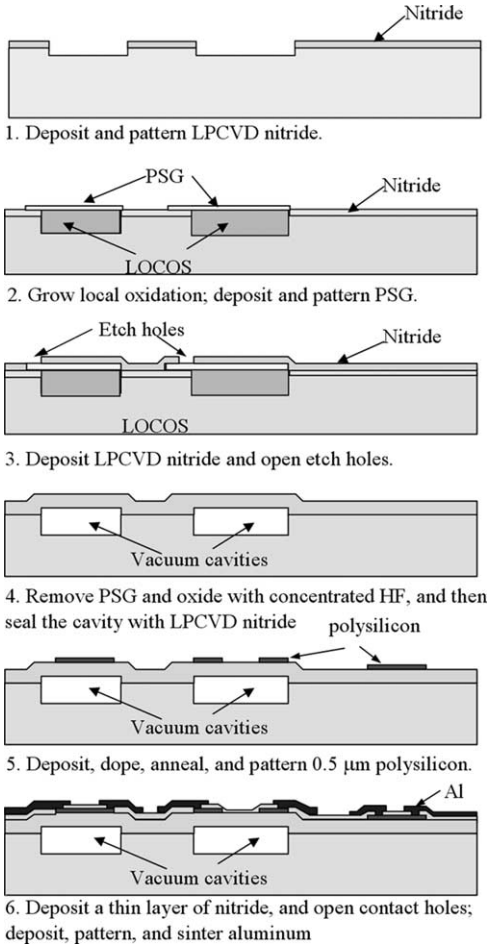

Fig. 3. Simplified fabrication process of one sensor cluster.

they have different doping concentrations, different patterns and locations, and different functions. For shear-stress sensors and temperature sensors, the polysilicon is employed as temperature sensitive resistors and is heavily doped. With a doping concentration of $2 \times 10^{20}\,cm^{-3}$, the temperature coefficient of resistance of polysilicon is about 0.1% °C^{-1}. For pressure sensors, the polysilicon is employed as a piezoresistive material and is lightly doped. With a boron concentration of $2 \times 10^{19}\,cm^{-3}$, the gauge factor of polysilicon is about 30 [16]. Higher boron concentration will lead to smaller gauge factor. Another good reason to choose this concentration for pressure sensors is that the polysilicon resistor has a nearly zero TCR at this doping level [16]. Thus, the temperature sensitivity of the pressure sensor can be minimized. After formation of polysilicon sensing elements, another 0.18 μm thick nitride layer is deposited as a passivation layer to prevent the drift of the polysilicon resistors from thermal oxidation in air [19]. The contact holes are then opened and aluminum is evaporated, patterned, and sintered (at 450 °C in N_2) to form metal wires. Finally, the multi-sensor chip is diced into 2 cm × 1 cm chips and Fig. 4 shows one sensor cluster and a complete multi-sensor chip. Note that the fabrication processes for the shear-stress and

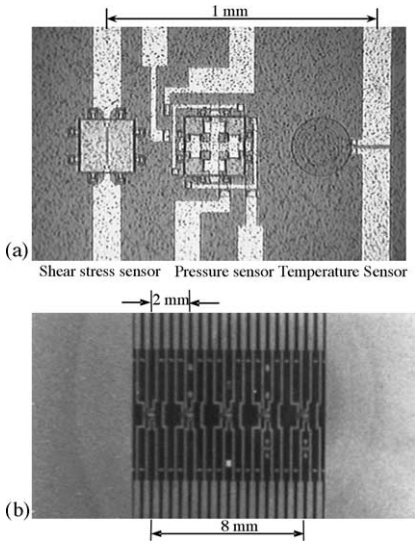

Fig. 4. (a) Micrograph of one sensor cluster. (b) Micrograph of a multi-sensor chip containing five sensor clusters.

pressure sensors are almost identical. Therefore, the fabrication of the multi-sensor chip is not significantly complicated compared with the fabrication of a single-sensor chip.

4. Testing and discussion

Fig. 5 shows the calibration curve of a typical pressure sensor on the multi-sensor chip. The vertical axis is the output voltage of the Wheatstone bridge formed by the polysilicon piezoresistors. The excitation voltage applied is 5 V. The normalized sensitivity is 82.9 μV/(kPa V). The sensitivities of other pressure sensors are between 82.1 μV/(kPa V) and 83.8 μV/(kPa V). Note that the output voltage at the atmospheric pressure is not zero. This is mainly due to the mismatch of the piezoresistors and the initial bending of the diaphragm caused by the atmospheric pressure.

The TCR of the heavily doped polysilicon (2×10^{20} cm^{-3}) has also been measured. Fig. 6 shows a typical resistance versus temperature curve. The TCR extracted from this curve is 0.104% $°C^{-1}$, which agrees well with published values [16].

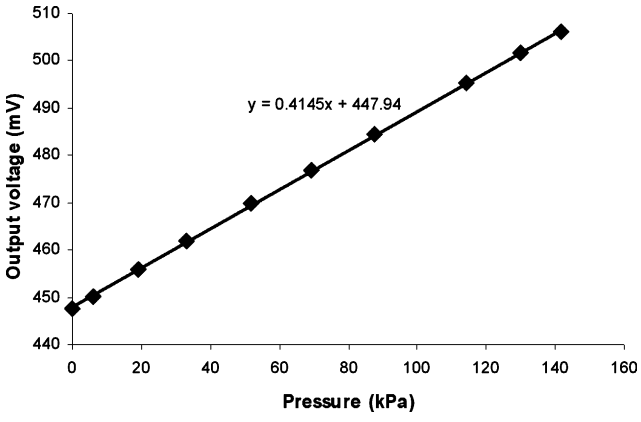

Fig. 5. The calibration curve of one pressure sensor on the multi-sensor chip.

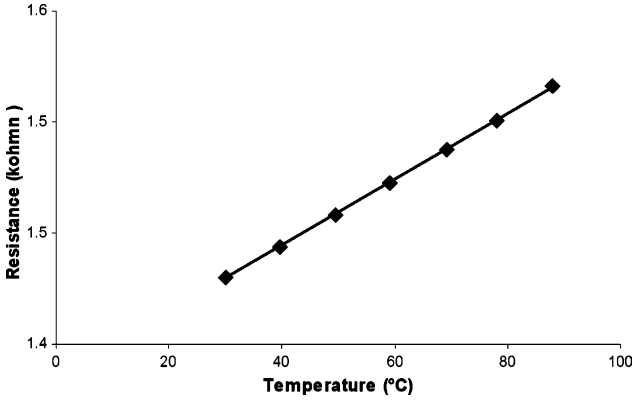

Fig. 6. Calibration of the TCR of heavily doped polysilicon (2×10^{20} cm^{-3}).

To demonstrate its capability to measure microchannel flows, the multi-sensor chip is first bonded to a printed circuit board and then another channel chip is flip-bonded on top of the sensor chip as shown in Fig. 7. The channel, with a rectangular uniform cross-section, is 2.5 mm wide, 18 mm long, and 200 μm high. Deep reactive ion etching (DRIE) is used to machine the channel and the inlet from the other side of the chip. The first sensor cluster is 4 mm away from the inlet to ensure all the sensors are in the fully developed flow region. Fig. 8 shows the pressure and temperature distributions of a fully developed laminar flow with a Mach number of 0.2. Mach number is defined as the ratio of flow speed to speed of sound. With a Mach number of 0.2 (equivalent to a mean flow velocity of 69 m/s), the flow is generally considered incompressible. The pitch of the sensors is 2 mm and the distance from the first sensor to the last one is 8 mm. As expected, the temperature is constant, while the pressure drops linearly along the channel.

It is also well known that in a fully developed laminar flow, the shear stress is constant. Fig. 8(c) shows that the five shear-stress sensors give nears identical readings of $\Delta V/V_0$, where ΔV is the voltage change and V_0 is the output voltage

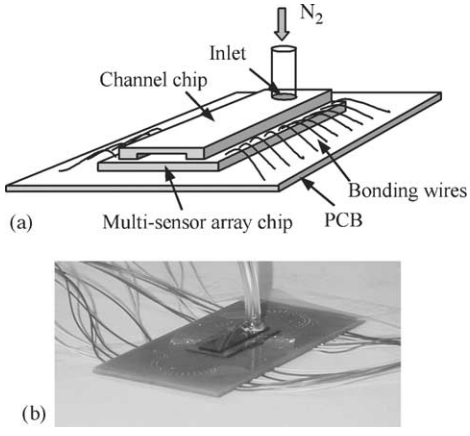

Fig. 7. (a) Schematic and (b) photograph of the packaged device.

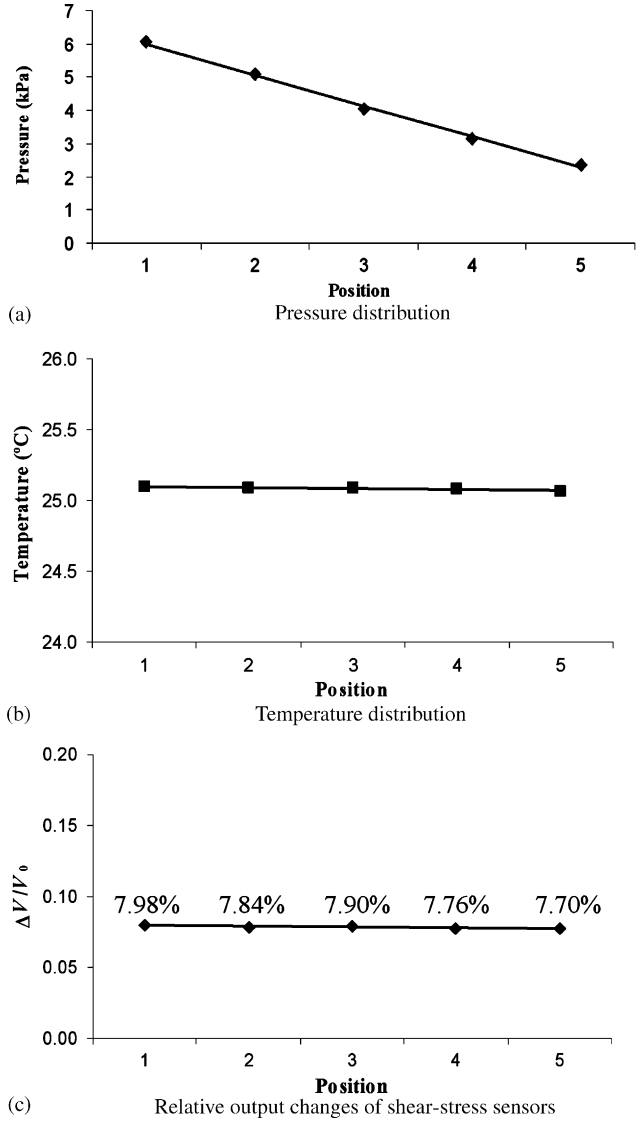

Fig. 8. Measurement of a fully developed incompressible channel flow with a Mach number of 0.2. (a) Pressure distribution; (b) temperature distribution; (c) relative output changes of shear-stress sensors.

at zero shear-stress. All the shear stress sensors are operated at an over-heat ratio of 10%. It is worth noting that the properties of different shear-stress sensors exhibit some variations due to limitations in the control of the fabrication process. For example, the electrical resistance may be slightly different from sensor to sensor, and errors may occur when setting the over-heat ratios. These factors will contribute to the sensitivity variations of the shear-stress sensors. To address this issue, we use a simple normalization method to minimize the variation to a first order approximation. Replacing V in Eq. (3) with $V_0 + \Delta V$ yields

$$\frac{{V_0}^2 + 2\Delta V V_0 + \Delta V^2}{R_S} = \Delta T A_t (\rho\tau)^{1/n} + \Delta T B_t \quad (7)$$

At zero shear stress, there exists the following relationship:

$$\frac{V_0^2}{R_S} = \Delta T B_t \quad (8)$$

Thus, Eq. (7) is simplified to

$$\frac{2V_0\Delta V}{R_S} + \frac{\Delta V^2}{R_S} = \Delta T A_t (\rho\tau)^{1/n} \quad (9)$$

Dividing both sides of Eq. (9) with ${V_0}^2/R_S$, and neglecting $(\Delta V/V_0)^2$ by assuming $\Delta V/V_0 \ll 1$, we finally get

$$\frac{\Delta V}{V_0} = \frac{A_t}{2B_t}(\rho\tau)^{1/n} \quad (10)$$

Eq. (10) clearly states that $\Delta V/V_0$ is independent of R_S. Namely, by normalizing ΔV to V_0, the influence of R_S on the sensitivity can be eliminated. In the mean time, the average temperature difference ΔT is also cancelled out and thus the influence of over-heat ratios is reduced significantly as well. This is the reason why the vertical axis of Fig. 8(c) is $\Delta V/V_0$ instead of ΔV. The $\Delta V/V_0$ offers a better sensor-to-sensor uniformity (with a variation $< \pm 1.8\%$) compared with the variation of ΔV ($\pm 4.5\%$). Note that even the $\pm 4.5\%$ variation of ΔV is not significant, and this is made possible by the following approaches. First, the five shear-stress sensors are on the same chip and thus have almost matched parameters. For example, the variation of the sensor resistance is $< \pm 1.7\%$. Second, the over-heat ratios have been carefully adjusted to be accurate as possible. We have also investigated the effect of over-heat ratio by increasing its value of one sensor from 10% to 20%. ΔV increases from 0.462 V to 0.623 V, while $\Delta V/V_0$ only changes from 7.90% to 7.54%. The effectiveness of this normalization method can be clearly observed. From Eq. (10), it can also be observed that in constant temperature mode the normalized output is insensitive to the TCR of polysilicon. Note that the gas density ρ and viscosity μ are both functions of temperature, and therefore $\Delta V/V_0$ is still a weak function of the over-heat ratio. In addition, B_t is determined by the thermal resistance of the nitride diaphragm. Thus, the thermal resistance variation due to the non-uniformity of LPCVD nitride cannot be cancelled.

Compressible flow (with a Mach number of 0.6) has also been measured in the channel, as shown in Fig. 9. The slight increase of pressure gradient and the temperature drop along the channel, which are characteristic of a compressible channel flow, can be observed. Fig. 9(c) plots the output of shear-stress sensors. Note that the term $(\Delta V/V_0)^2$ is included since it is relatively large and cannot be neglected in this case. Except the first sensor, the remaining sensors indicate the increase of the shear stress along the channel. Note that the gas is injected into the channel vertically from a top inlet (Fig. 7), leading to a 3D flow distribution at the entrance. The flow at the location of the first sensor may not be fully developed. Further investigation is needed to explain the behavior of the first shear-stress sensor.

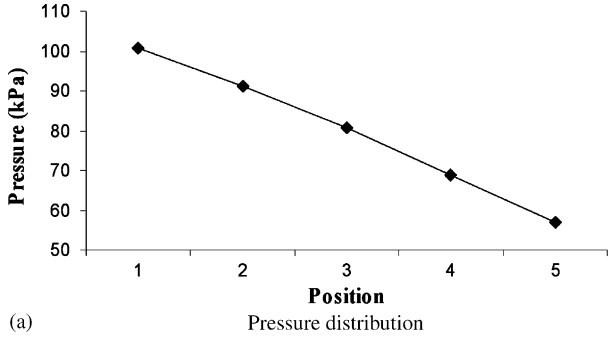

(a) Pressure distribution

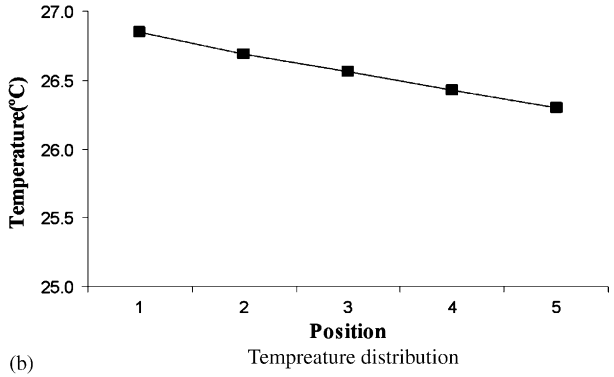

(b) Tempreature distribution

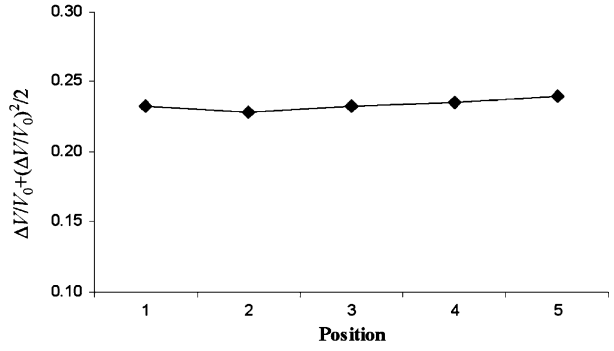

(c) Response of the shear-stress sensors.

Fig. 9. Measurement of a fully developed compressible channel flow with a Mach number of 0.6. (a) Pressure distribution; (b) temperature distribution; (c) response of the shear-stress sensors.

In addition to channel flow measurement, the multi-sensor chip bonded with a channel can also function as a flowmeter. Interestingly, two different flow rate measurement principles can be employed: differential pressure and thermal anemometry. For the rectangular channel flow, if the height h is much smaller than the width (which is true in our case), in the laminar flow regime the flow rate Q is given by [20]:

$$Q = \frac{h^3 w}{12\mu}\frac{\mathrm{d}p}{\mathrm{d}x} \tag{11}$$

Thus, the flow rate can be obtained by measuring the pressure gradient (or equivalently the pressure drop) along the channel. Fig. 10 plots the pressure difference Δp measured by pressure sensors #1 and #5 as a function of mass flow rate Q in both laminar and turbulent flow regimes. The mass flow rate is measured by a commercial mass flowmeter connected

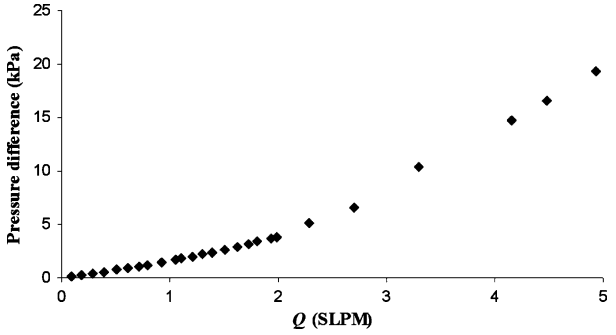

Fig. 10. Calibration of flowmeter based on differential pressure measurement (h = 200 μm and N_2 flow).

in series. The unit is standard litter per minute (SLPM). Note that 1 SLPM in our experimental setup is equivalent to a mean flow velocity of 33.3 m/s. The transition region from laminar to turbulent flow is near Q = 2.5 SLPM, corresponding to a Reynolds number of Re = 2100. The laminar flow data are linear and the slope agrees with that predicted by Eq. (11). Note the bending of the curve when the flow enters turbulent region, indicating that Eq. (11) is no longer valid in the turbulent flow regime.

Simultaneously, the flow rate can be measured using the shear-stress sensor based on thermal anemometry principle. The response of the thermal shear-stress sensor to nitrogen flow is shown in Fig. 11. The over-heat ratio a_R of the shear-stress sensor is 10%. One limitation of the hot-film shear-stress sensors is that the output is sensitive to ambient temperature. Using an on-chip temperature sensor, the experimental data have been temperature-compensated.

The principle of flow rate measurement using the shear-stress sensor is as follows. Based on force balance, the relationship between the wall shear stress (friction) τ and the pressure gradient dp/dx along the channel is given by [20]:

$$\tau = \frac{h}{2}\frac{\mathrm{d}p}{\mathrm{d}x} \tag{12}$$

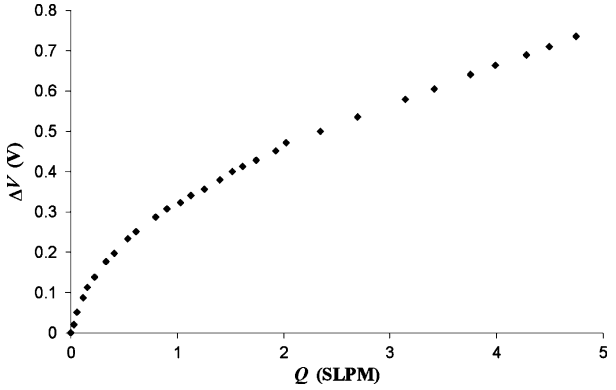

Fig. 11. Calibration of the flowmeter based on the thermal shear-stress sensor (h = 200 μm, a_R = 10%, and N_2 flow).

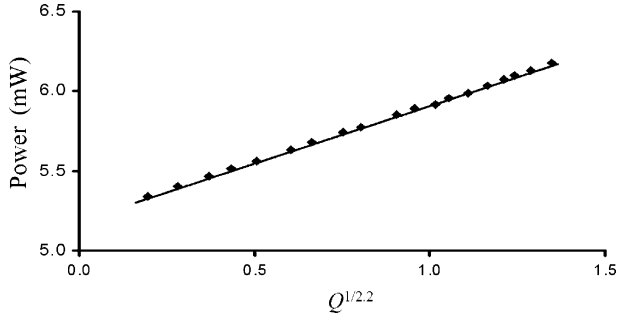

Fig. 12. Input power vs. $Q^{1/2.2}$ (laminar flow region).

Replacing the pressure gradient using Eq. (11), the shear stress in laminar flow region is given by:

$$\tau = \frac{6\mu}{h^2 w} Q \tag{13}$$

Thus, the relationship between the input power and the flow rate in laminar flow region is given by:

$$P = \frac{V^2}{R_S} = A_0 Q^{1/n} + B_0 \tag{14}$$

where $A_0 = \Delta T A_t \left(\frac{6\rho\mu}{h^2 w}\right)^{1/n}$ and $B_0 = \Delta T B_t$. If $\Delta V/V_0 \ll 1$, the above equation can be simplified to

$$\frac{\Delta V}{V_0} = \frac{A_0}{2B_0} Q^{1/n} \tag{15}$$

Thus, the relative output change can be used to reduce the sensitivity variations as well. Eq. (13) states that flow rate Q is proportional to wall shear stress τ in the laminar flow region. Thus, in the laminar flow region of Fig. 11, the horizontal axis can be readily converted to shear stress, resulting in a calibration curve for the shear-stress sensor.

Using the least squares method to fit the laminar flow data, we obtain $n = 2.2$, which differs from the conventional value of 3. Fig. 12 re-plots the laminar flow part of Fig. 11 by changing the horizontal axis to $Q^{1/2.2}$. For one time, the classical law with n of 3 has been used to characterize the micromachined shear-stress sensors. However, experimental data clearly indicate that the classical hot-film theory, stating that the heat removed by the flow is proportional to $\tau^{1/3}$, needs to be modified for the MEMS shear-stress sensors. This is mainly because the assumption that the thermal boundary layer is very thin compared to the dimension of heated area is not valid anymore. More detailed investigation of this problem can be found in [21].

In order to fully understand the characteristics of the flow rate measurement using shear-stress sensors, extensive tests have been carried out with different over-heat ratios, channel heights and gases. Table 1 compares A_0 and B_0 extracted from the experimental data for different over-heat ratios in the 200 μm high channel for both nitrogen and helium flows. An averaged value of $n = 2.20$ is used for all the data fittings.

Table 1
Experimental A_0 and B_0 for different a_R ($h = 200$ μm and $n = 2.20$)

Gas	Over-heat ratio (%)	A_0	B_0
Nitrogen	5	0.349	2.84
	10	0.719	5.20
	20	1.31	9.52
Helium	5	0.706	3.64
	10	1.31	6.87
	20	2.30	13.0

From the above table, we can clearly see that when the over-heat ratio doubles, A_0 and B_0 approximately double correspondingly. This can be explained by the following analysis. We know that the resistance of the sensing element at temperature T is

$$R_S = R_{S0}[1 + \alpha_T(T - T_0)] \tag{16}$$

where R_{S0} is the resistance at reference temperature T_0 and α_T is the TCR of the sensing element. Combined with Eqs. (4) and (16), the over-heat ratio is given by

$$a_R = \alpha_T \Delta T \tag{17}$$

A_0 and B_0 are both proportional to ΔT (note that this is only approximately true because the gas density ρ and viscosity μ are weak functions of the temperature) and hence are proportional to the over-heat ratio a_R. Table 2 shows experimentally determined values of A_0 and B_0 for different channel heights with a constant over-heat ratio of 10% for both nitrogen and helium flows. From Eq. (14), we have $A_0 \propto h^{-2/n}$. According to Table 2, A_0 increases as h decreases, but in a way that is different from this power-law dependence. This might be attributed to the fact that changes in h also influence heat transfer in the channel, which needs to be further investigated.

Gas properties will also impact the sensor sensitivity. It can be shown that $A_0 \propto k_T \alpha^{-1/n}$, where $\alpha = k_T/\rho c_P$ is the thermal diffusivity of the gas. For nitrogen, $k_T = 2.59 \times 10^{-2}$ W/(m K) and $\alpha = 2.21 \times 10^{-5}$ m^2/s, and for helium, $k_T = 0.152$ W/(m K) and $\alpha = 1.80 \times 10^{-4}$ m^2/s. Let n be 2.20, we obtain that the ratio of A_0 (He) over A_0 (N_2) is 2.26. From Tables 1 and 2, we can see that all the experimental ratios are smaller than this value, which also needs to be further investigated. It is also observed that B_0 in helium gas is always larger than it is in nitrogen gas. This indicates that at zero flow, the heat loss through the ambient gas is not negligible.

Table 2
Experimental A_0 and B_0 for different channel heights ($a_R = 10\%$ and $n = 2.20$)

Gas	Channel height (μm)	A_0	B_0
Nitrogen	150	0.789	5.61
	200	0.719	5.20
	288	0.562	5.48
Helium	150	1.51	7.25
	200	1.31	6.87
	288	0.847	7.38

Flow sensings by pressure and shear-stress measurements generally complement each other. As we can see, the thermal flowmeter has a very high sensitivity, although the output is not a linear function of flow rate. In Fig. 11, at $Q = 1$ SLPM, the sensitivity is 0.17 V/SLPM while at $Q = 0.1$ SLPM, it increases to 0.62 V/SLPM. This type of flowmeter has extremely high sensitivity at small flow rates, which is desirable for some microfluidic applications. The drift due to its elevated operating temperature is a concern. On the other hand, the flowmeter based on differential pressure principle is less sensitive to ambient temperature and has a simple linear relationship between the pressure drop and flow rate. But its sensitivity is low compared with the thermal flowmeter. To obtain high sensitivity, a large pressure drop across the channel needs to be generated. This is not allowed for many microfluidic applications.

There are several aspects in which the multi-sensor chip can be further improved. In this work, the temperature sensors are made directly on the substrate. It would be advantageous to implement a thermal isolation structure to reduce the effect of the substrate on the temperature measurement. The shear-stress sensors exhibit some pressure sensitivity (0.27–0.21 mV/kPa). This is because heavily doped polysilicon is piezoresistive (with a longitudinal gauge factor of ∼20) [16]. The pressure sensitivity can be reduced by adjusting the length of the polysilicon resistor, and making a more rigid diaphragm. More detailed information on this issue can be found in [22]. After coating a waterproof layer, such as low temperature oxide (LTO) or parylene C, this multi-sensor chip can be used to measure liquid flows. Of course, this sensor chip can also be employed to measure flows on open surfaces although in this paper only channel flow measurements are reported.

5. Conclusions

A multi-sensor chip that contains five sensor clusters arranged in a 1D array has been successfully developed. Every sensor cluster consists of one shear-stress sensor, one pressure sensor, and one temperature sensor. Thin film polysilicon was employed as the sensing elements for all three sensors. The multi-sensor chip's capability to study some complex channel flows such as flows in micro nozzles has been demonstrated by the successful measurement of incompressible and compressible channel flows. By normalizing ΔV to V_0, the variations of shear-stress sensitivity caused by the variations of electrical resistance and over-heat ratio can be reduced. Flow rate measurements based on both differential pressure and thermal anemometry principles have been demonstrated. We also confirmed that the classic law for conventional hot-film sensors, which states that the heat removed by the flow is proportional to $\tau^{1/3}$, is not valid for the micromachined shear-stress sensors. Extensive tests have been carried out on the shear-stress sensor with various over-heat ratios, channel heights and gases, resulting in several useful conclusions.

Acknowledgment

This work was supported by Jet Propulsion Laboratory under account code 49-204-52000-0-3460.

References

[1] G.T.A. Kovacs, Micromachined Transducers Sourcebook, WCB McGraw-Hill, 1998.
[2] R.S. Muller, R.T. Howe, S.D. Senturia, R.L. Smith, R.M. White, Microsensors, IEEE Press, New York, 1991.
[3] W.S. Trimmer, Micromechanics and MEMS: Classic and Seminar Papers to 1990, IEEE Press, 1997.
[4] J. Liu, Y.C. Tai, K. Pong, C.M. Ho, MEMS for pressure distribution studies of gaseous flows in microchannels, in: Presented at the Eighth IEEE International Conference on Micro Electro Mechanical Systems (MEMS), Amsterdam, the Netherlands, January 29–February 2, 1995, pp. 209–215.
[5] L. Zhang, J.M. Koo, L. Jiang, M. Asheghi, K.E. Goodson, J.G. Santiago, T.W. Kenny, Measurements and modeling of two-phase flow in microchannels with nearly constant heat flux boundary conditions, J. Microelectromech. Syst. 11 (2002) 12–19.
[6] L. Jiang, M. Wong, Y. Zohar, Phase change in microchannel heat sink under forced convection boiling, in: Presented at IEEE International Conference on Micro Electro Mechanical Systems (MEMS), Miyazaki, Japan, January 23–27, 2000, pp. 397–402.
[7] M.A. Schmit, R.T. Howe, S.D. Senturia, J.H. Haritonidis, Design and calibration of a microfabricated floating-element shear-stress sensor, IEEE Trans. Electron Devices 35 (1988) 750–757.
[8] J. Shajii, K.-Y. Ng, M.A. Schmidt, A microfabricated floating-element shear-stress sensor using wafer-bonding technology, J. Microelectromech. Syst. 1 (1992) 89–94.
[9] A. Padmanabhan, H.D. Goldberg, K.S. Breuer, M.A. Schmidt, Silicon micromachined floating-element shear-stress sensor with optical position sensing by photodiodes, in: Presented at International Conference on Solid-State Sensors and Actuators, and Eurosensors IX, Stockholm, Sweden, June 25–29, 1995, pp. 436–439.
[10] T. Pan, D. Hyman, M. Mehregany, E. Reshotko, B. Willis, Characterization of microfabricated shear-stress sensors, in: Presented at International Conference on Solid-State Sensors and Actuators, and Eurosensors IX, Stockholm, Sweden, June 25–29, 1995, pp. 443–446.
[11] T.J. Hanratty, J.A. Campbell, Measurement of wall shear-stress, in: R.J. Goldstein (Ed.), Fluid Mechanics Measurements, second ed., Taylor & Francis, 1996, pp. 575–648.
[12] C. Liu, Y. C. Tai, J. B. Huang, and C. M. Ho, Surface micromachined thermal shear-stress sensor, in: Presented at ASME International Mechanical Engineering Congress and Exposition, Chicago, Illinois, November 6–11, 1994, pp. 9–15.
[13] F. Jiang, Y.C. Tai, B. Gupta, R. Goodman, S. Tung, J.B. Huang, C.M. Ho, A surface-micromachined shear-stress imager, in: Presented at IEEE International Conference on Micro Electro Mechanical Systems (MEMS), San Diego, California, February 11–15, 1996, pp. 110–115.
[14] Y. Xu, F. Jiang, S. Newbern, A. Huang, C.-M. Ho, Y.-C. Tai, Flexible shear-stress sensor skin and its application to unmanned aerial vehicles, Sens. Actuators A: Phys. 105 (2003) 321–329.
[15] R.J. Goldstein, Fluid Mechanics Measurements, second ed., Taylor & Francis, 1996.
[16] V. Mosser, J. Suski, J. Goss, E. Obermeier, Piezoresistive pressure sensors based on polycrystalline silicon, Sens. Actuators A: Phys. 28 (1991) 113–132.
[17] J. Liu, Integrated micro devices for small scale gaseous flow study, Ph.D. Thesis, California Institute of Technology, Pasadena, 1995.

[18] M. Sekimoto, H. Yoshihara, T. Ohkubo, Silicon-nitride single-layer X-ray mask, J. Vac. Sci. Technol. 21 (1982) 1017–1021.
[19] K.C. Saraswat, H. Singh, Thermal-oxidation of heavily phosphorus-doped thin-films of polycrystalline silicon, J. Electrochem. Soc. 129 (1982) 2321–2326.
[20] F.M. White, Fluid Mechanics, second ed., McGraw-Hill, 1986.
[21] Q. Lin, F. Jiang, X.-Q. Wang, Y. Xu, Z. Han, Y.-C. Tai, J. Lew, C.-M. Ho, Experiments and simulations of MEMS thermal sensors for wall shear-stress measurements in aerodynamic control applications, J. Micromech. Microeng. 14 (2004) 1640–1649.
[22] Y. Xu, F. Jiang, Q. Lin, J. Clendenen, S. Tung, Y.-C. Tai, Underwater shear-stress sensor, in: Presented at IEEE International Conference on Micro Electro Mechanical Systems (MEMS), Las Vegas, Nevada, January 20–24, 2002.

Biographies

Yong Xu received his BS degree in electronics engineering from Tsinghua University, Beijing, in 1997, and the MS and PhD degrees in electrical engineering from the California Institute of Technology, Pasadena, in 1998 and 2002, respectively. He is currently an assistant professor in the Department of Electrical and Computer Engineering at Wayne State University. His research interests include MEMS smart skin technology, microfluidics, physical and biological sensors, novel packaging technology, and nanotechnology.

Chen-Wei Chiu received his BS degree in mechanical engineering from National Taiwan University in 1994, and the MS degree in mechanical engineering from University of California, Los Angeles, in 1998. After receiving the MS degree, he worked in Umachines Inc., a Caltech based startup, as a MEMS engineer specialized in MEMS sensors and optical switches. He is currently a MEMS project manager in Wistron Corp., a major international EMS provider in Taiwan.

Fukang Jiang received his BS degree in physics from Hangzhou University, PRC, in 1984 and MS and PhD degree in electrical engineering from the California Institute of Technology in 1992 and 1998, respectively. He is currently with Umachines Inc. His current interest is in the development of MEMS sensors and actuators for industrial applications.

Qiao Lin received his PhD in mechanical engineering from Caltech in 1998. His thesis research involved automated planning of robotic manipulation, with an emphasis on kinematics and mechanics of compliant grasps and fixtures. Dr. Lin conducted postdoctoral research in microelectromechanical systems (MEMS) at the Caltech Micromachining Laboratory from 1998 to 2000, and has since been an assistant professor in the Department of Mechanical Engineering at Carnegie Mellon University. His research interests are in MEMS, including micro/nano-fluidic, thermal, and robotic devices for biomedical applications.

Yu-Chong Tai received his BS degree from National Taiwan University, and the MS and PhD degrees in electrical engineering from the University of California at Berkeley in 1986 and 1989, respectively. After Berkeley, he joined the faculty of electrical engineering at the California Institute of Technology and built the Caltech Micromachining laboratory. He is currently a full professor of electrical engineering at Caltech. His research interests include flexible MEMS, integrated microfluidics, neuroprobes and chips, optical MEMS and biochemical sensors. He has received several awards such as the IBM Fellowship, the Best Thesis Award, the Presidential Young Investigator (PYI) Award and the David and Lucile Packard Fellowship. He co-chaired the 2002 IEEE MEMS Conference in Las Vegas. He is currently a subject editor of the Journal of MEMS. He's also a section editor of Sensors and Actuators.